OPEN ACCESS

Applied Physics Express 17, 086501 (2024) LETTER

https://doi.org/10.35848/1882-0786/ad64ba

Formation of GaN mesas with reverse-tapered edge structures on a lattice-matched AlInN layer for a positive beveled edge termination

Takayoshi Oshima*, Masataka Imura, and Yuichi Oshima

Research Center for Functional Materials, National Institute for Materials Science, Tsukuba, Ibaraki 305-0044, Japan

*E-mail: OSHIMA.Takayoshi@nims.go.jp

Received June 26, 2024; revised July 15, 2024; accepted July 17, 2024; published online July 31, 2024

GaN mesas were fabricated by sequential dry and wet etching of a $+c$-oriented GaN layer onto a lattice-matched AlInN layer for future applications of positive beveled edge termination, which is desirable for preventing premature breakdown of power devices. The dry etching produced hexagonal AlInN/GaN mesas surrounded by m-plane sidewalls with six protrusions at the vertices. The subsequent hot phosphoric acid etching selectively etched the AlInN layer to expose and etch the chemically unstable $-c$ surface of the GaN layer, which formed reverse-tapered $\{10\bar{1}\bar{2}\}$ facets. The protrusions were sacrificed during the wet etching to prevent undesirable positive tapering at the vertices.

In the field of power electronics, GaN is a crucial material owing to its superior electrical properties such as a wide bandgap, high electron mobility, and high breakdown voltage,[1] which empower GaN devices to operate at elevated voltages, frequencies, and temperatures compared to Si counterparts. Thus, GaN power devices are well-suited for diverse applications such as power converters, radiofrequency amplifiers, and electric vehicle inverters.[2–4]

A major design consideration for GaN power devices is edge termination. Managing the electric field distribution at the edges of a device is necessary to prevent premature breakdown and ensure reliable operation.[5] Thus far, termination structures such as field plates, field-limiting rings, and junction termination extensions have been employed.[6–9] However, sharp electric field gradients persist at the edges of the dielectric plate and near the p–n junction, and these termination structures require deposition, implantation, and patterning steps that increase manufacturing costs. Consequently, an edge termination that addresses these drawbacks is potentially necessary.

A positive beveled edge termination is a viable solution to the problems faced by current termination structures because it gradually decreases the electric field strength toward the edge of the device, which prevents localized high electric fields.[10,11] Furthermore, a beveled edge termination is cost-effective because it can be fabricated by etching only. Basically, there are two types of beveled edge terminations: positive and negative beveled edge terminations. In the positive beveled edge termination, more material is removed from the edge when progressing from the heavily doped side to the lightly doped side of the junction, or the junction area is linearly decreasing when going from the heavily-doped side to the lightly-doped side. While, in the negative beveled edge termination, more material is removed from the edge when progressing from the lightly doped side to the heavily doped side of the junction, or the junction area is linearly decreasing when going from the lightly-doped side to the heavily-doped side.[10,11] Theoretically, the positive beveled edge termination demonstrates a superior ability to reduce electric field at the edge compared to the negative beveled edge termination.[10] However, fabricating a positive beveled edge termination is challenging because most vertical power devices, such as Schottky barrier diodes, PN junction diodes, have a voltage-sustaining junction near the surface, where a lightly doped layer is on the lower side.[5] Hence, the implementation of positive beveled edge terminations for these devices requires the establishment of a reverse tapering process.

In the case of GaN, a reverse-tapered structure can be fabricated by utilizing its crystallographic nature. Stocker et al. achieved reverse tapering of c-oriented GaN on an AlN underlying layer by combining dry etching and material-/facet-selective wet etching.[12] The dry etching exposes the m-plane sidewalls of the GaN and AlN layers, and the subsequent wet etching in H_3PO_4 or KOH selectively etches the sides of the AlN layer while simultaneously undercutting the GaN layer to expose the etching-sensitive $-c$ side to create reverse-tapered sidewalls of etching-resistant $\{10\bar{1}\bar{2}\}$ or $\{10\bar{1}\bar{1}\}$ facets, respectively. Several studies have validated the efficacy of this technique for optical applications.[13–15] However, the AlN layer compromises the performance of power devices because of its lattice mismatch with GaN, which degrades the crystallinity of GaN. In addition, the low-doping capability of the AlN layer increases the series resistance of the device. For practical application in power devices, AlN should be replaced by a semiconductor with a weaker wet-etching resistance than GaN, the same in-plane lattice constant as GaN, and a higher doping capability than AlN.

The above criteria can be satisfied by using an AlInN layer instead of the AlN layer. AlInN achieves a lattice match with GaN at an In composition of ~18%.[16] Moreover, lattice-matched AlInN layers sandwiched with GaN layers can be etched selectively via electrochemical oxidation and/or hot nitric acid etching to create lateral air gaps between GaN layers to realize diffuse Bragg reflectors.[17–20] Furthermore, the carrier concentration of AlInN can be increased up to $\sim 10^{19}\,\mathrm{cm}^{-3}$ by Si and Ge doping.[21,22] The specific contact resistance at the AlInN/GaN interface is as low as $1.5 \times 10^{-7}\,\Omega\,\mathrm{cm}^2$,[21] and the vertical direction resistivity of a 300 nm thick AlInN layer is as low as $5.8 \times 10^{-4}\,\Omega\mathrm{cm}^2$.[22] These attributes make AlInN a desirable candidate as a side-etching layer material to initiate the formation of reverse tapered edge of GaN for power devices applications.

In this study, we used the above etching technique to fabricate hexagonal GaN mesas with reverse-tapered edges on a lattice-matched AlInN layer. Although some ingenuity was

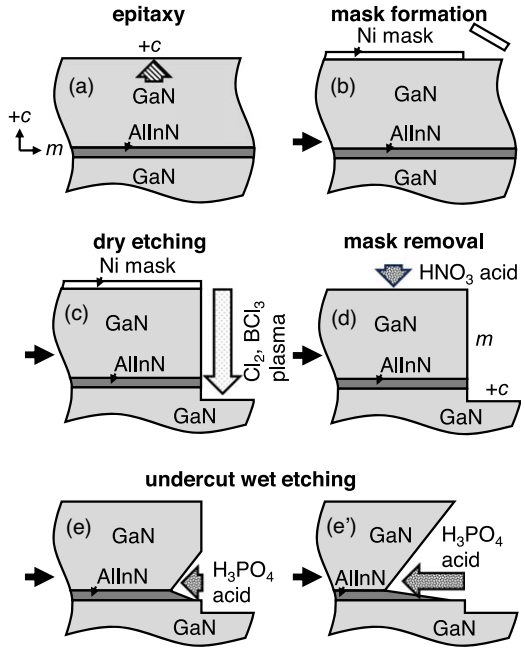

Fig. 1. Schematic for the process flow of forming reverse-tapered GaN sidewalls: (a) GaN/AlInN/GaN epitaxy, (b) Ni mask formation, (c) Cl_2/BCl_3 dry etching, (d) Ni mask removal, and (e) initial and (e') final stages of undercut wet etching in hot H_3PO_4 acid.

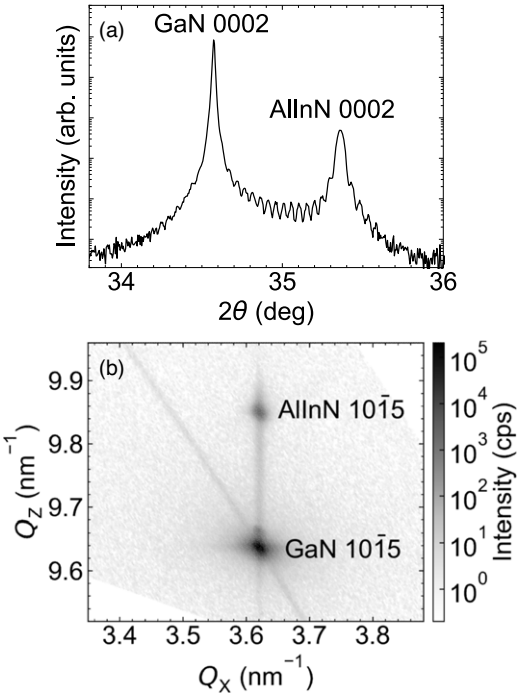

Fig. 2. X-ray diffraction: (a) θ–2θ pattern of 0002 peaks and (b) reciprocal space map in the vicinity of the 10$\bar{1}$5 spots of the GaN/AlInN/GaN multilayers.

necessary at the vertices, we successfully achieved reverse tapering around the entire circumference of the hexagonal mesa.

Figure 1 shows the steps of the entire process, which comprise GaN/AlInN/GaN epitaxy on a sapphire wafer [Fig. 1(a)], formation of a Ni mask for dry etching [Fig. 1(b)], dry etching using Cl_2 and BCl_3 plasma [Fig. 1(c)], removal of the Ni mask [Fig. 1(d)], and undercutting by wet etching using hot H_3PO_4 acid [Figs. 1(e) and 1(e')].

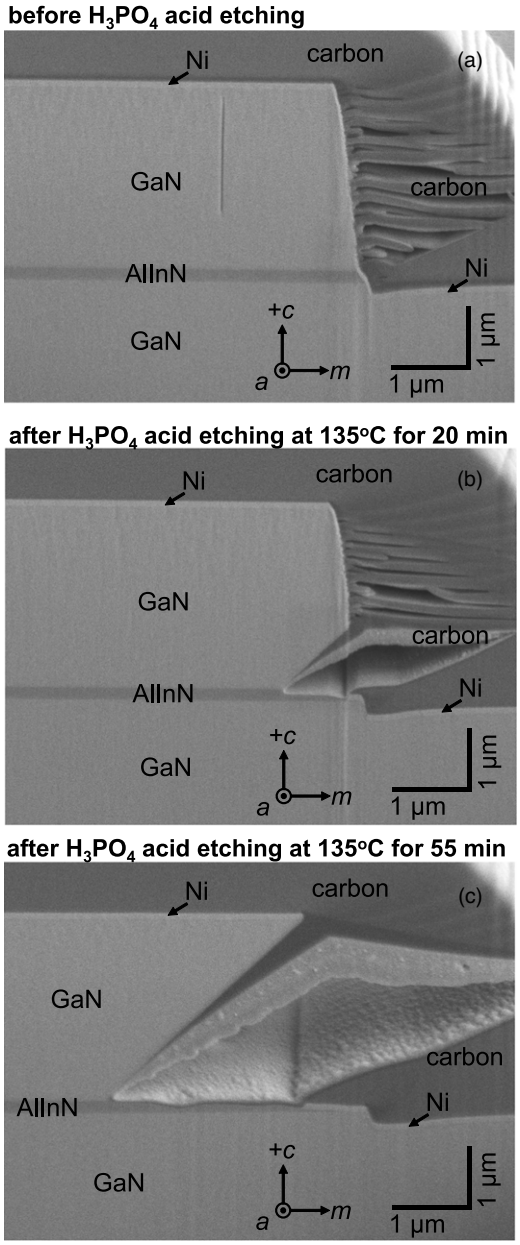

Fig. 3. Cross-sectional scanning electron microscopy images showing undercut etching of $+c$-oriented GaN on a lattice-matched AlInN layer. The images were taken (a) before etching and after (b) 20 min and (c) 55 min of wet etching in H_3PO_4 acid at 135 °C. Sectioning was done at the middle of one side of a hexagon using focused ion beam milling. The observed Ni and carbon layers are conductive and protective layers for the milling. The electron beam incidence was tilted by 54° with respect to the surface normal.

A GaN/AlInN/GaN stack was prepared on a 2-in c-plane sapphire wafer by metalorganic vapor phase epitaxy using standard growth recipes [Fig. 1(a)]. The thicknesses of the bottom GaN, AlInN, and top GaN layers were 2.83, 0.19, and 2.83 μm, respectively, which were measured by focused ion beam milling (FIB) and scanning electron microscopy (SEM). The epitaxial structures of the GaN/AlInN/GaN layers were investigated by X-ray diffraction using a monochromatic $CuK_{\alpha 1}$ radiation. In the θ–2θ wide scan (not shown), only (0001) oriented peaks of GaN and AlInN layers appeared except for those of the substrate, and no other orientation or phase peaks were detected. Laue fringe peaks of the AlInN layer were clearly observed [Fig. 2(a)], which indicated its high crystallinity and abrupt AlInN/GaN and

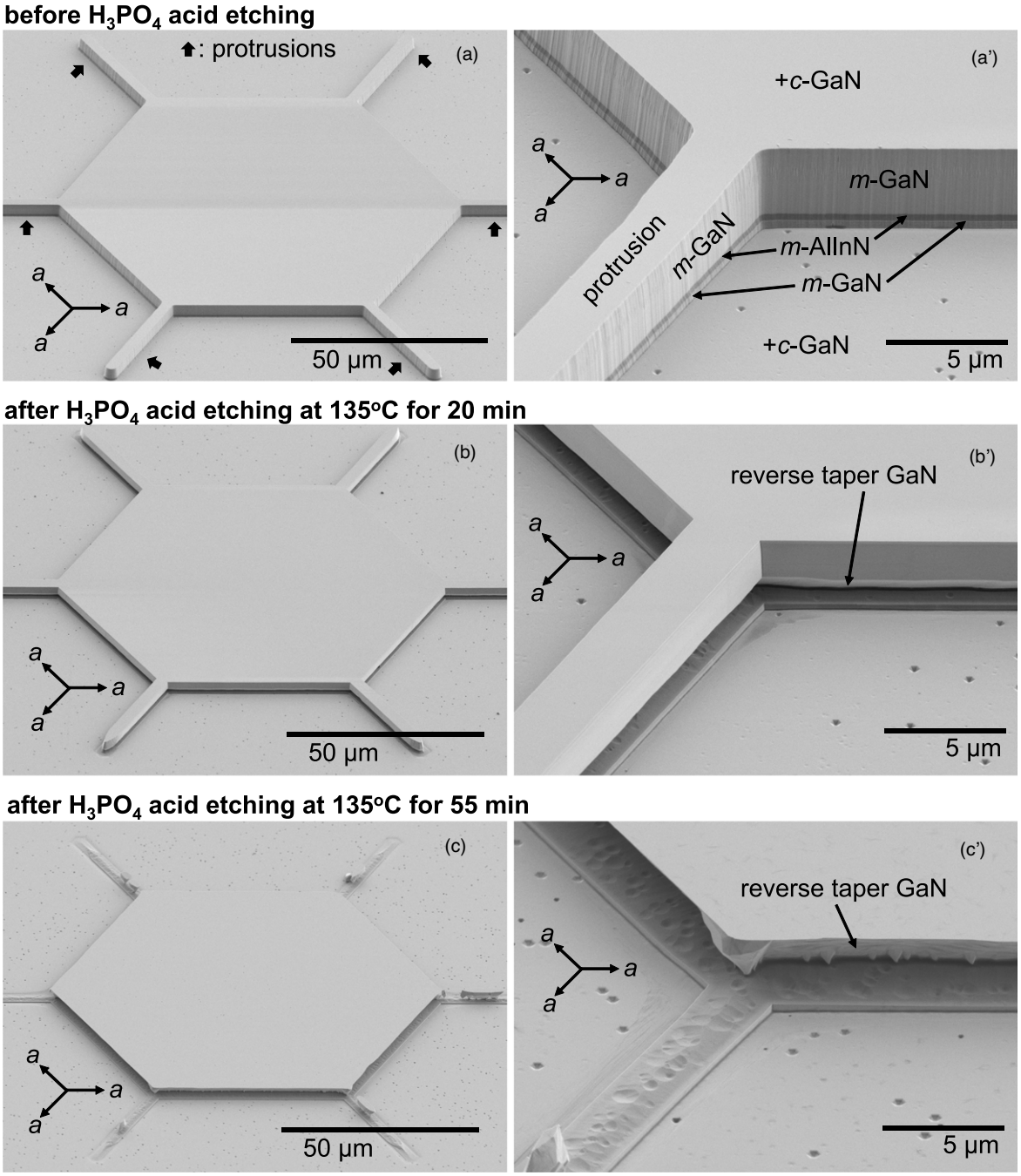

Fig. 4. Bird's-eye view scanning electron microscopy images showing the formation of hexagonal GaN mesas with reverse-tapered sidewalls. The images were taken (a) before etching and after (b) 20 min and (c) 55 min of wet etching in H_3PO_4 acid at 135 °C. (a'), (b'), and (c') are images corresponding to the vertices in (a), (b), and (c), respectively.

GaN/AlInN interfaces. Based on the fringe peak angles, the thickness of the AlInN layer was calculated as 195 nm. The reciprocal space map in the vicinity of $10\bar{1}5$ spots revealed that the AlInN and GaN spots had the same Q_X values [Fig. 2(b)], which means that the AlInN layer was fully strained to the GaN layers. Under the assumption of in-plane lattice matching, the In composition of the AlInN layer was estimated as 14.6% based on the main peak angle in the θ–2θ pattern, which is as described in the literature.[23)]

On the surface of the top GaN layer, a patterned Ni mask with a thickness of 200 nm was prepared by standard laser lithography, electron beam evaporation, and liftoff processes [Fig. 1(b)]. The Ni mask was in the shape of a regular hexagon with six protrusions at the vertices. All sides of the mask shape were aligned with the a directions (i.e. $[11\bar{2}0]$, $[1\bar{2}10]$, and $[\bar{2}110]$). Each side of the hexagon had a length of 50 μm while the protrusions had a length and width of 30 and 2 μm, respectively. The necessity of the protrusions will be discussed later. Dry etching was performed with the patterned Ni mask to access the m-plane sidewalls of the top GaN and AlInN layers [Fig. 1(c)]. The etching was conducted in Cl_2 and BCl_3 plasma[24)] at gas flow rates of 45.0 and 5.0 sccm, respectively, and a chamber pressure of 0.5 Pa. The inductively coupled plasma and bias power inputs were 300 and 200 W, respectively. Under these conditions, the typical etching rate for $+c$-GaN was 0.27 μm min^{-1}. The etching reached the top part of the bottom GaN layer, which exposed the m-plane surfaces of the top GaN and AlInN layers. The Ni mask was removed

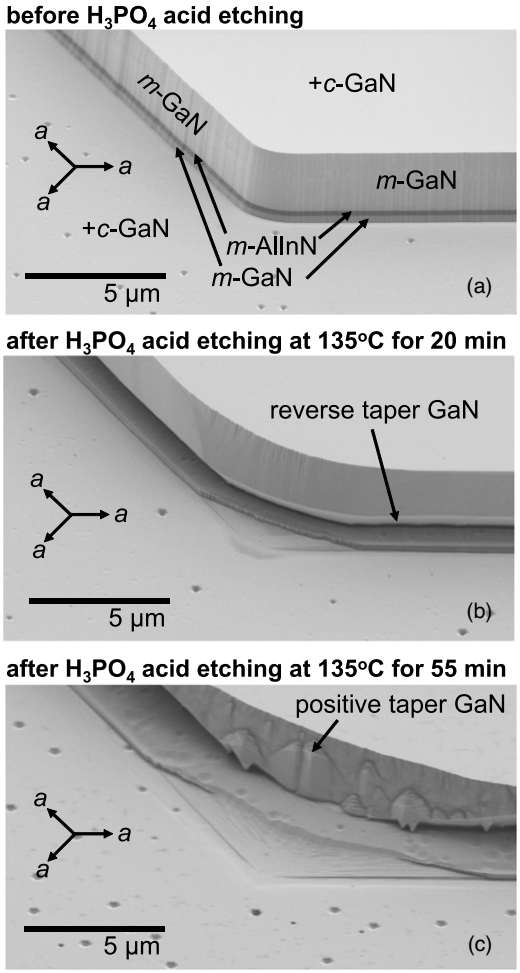

Fig. 5. Bird's-eye view scanning electron microscopy images showing erosion at vertices of hexagonal GaN mesas fabricated without protrusions. The images were taken (a) before etching and after (b) 20 min and (c) 55 min of wet etching in H_3PO_4 acid at 135 °C.

by immersing the sample in nitric acid at room temperature [Fig. 1(d)]. The dry-etched structures remained intact in this process as evidenced by tilted-view cross-sectional and surface SEM images [Figs. 3(a), 4(a) and 4(a')].

Finally, undercutting was conducted to create reverse-tapered GaN structures [Figs. 1(d) and 1(e)] by wet etching in hot phosphoric acid, which was stirred and heated at 135 °C in a glass beaker using a hot plate stirrer. The process temperature was monitored and controlled by using a Teflon-coated thermocouple immersed in the acid. Etching times of 20 and 55 min were used for different samples.

The etching predominantly progressed at the AlInN/GaN interface. Figures 3(b) and 3(c) show cross-sectional SEM images after wet etching for 20 and 55 min, respectively. When the top part of the AlInN was side-etched, the exposed back side of the top GaN layer was immediately etched to form reverse-tapered facets. The second GaN etching process was much faster than that of the AlInN layer. Accordingly, the facet structure was maintained for the etched GaN surface throughout the etching process, and the lateral position of the facet was constrained to the inner end for the undercut etching. The face angle between the top surface and reverse-tapered facet was ~48°, which is closer to the calculated value of 43.2° for the $\{10\bar{1}2\}$ facet than 62.0° for the $\{10\bar{1}1\}$ facet using the lattice parameters of GaN.[25] Therefore, the observed facet was likely to be $\{10\bar{1}2\}$. The slight angle difference of ~5° can be attributed to deviations in the holder normal direction and Ga beam and electron beam directions of the used FIB-SEM system. The mechanism of the undercut etching was almost the same as that of the etching process at the AlN/GaN interface.[12] However, most of the AlInN layer remained at the inner end with undercut etching because it has a higher chemical stability than AlN. Thus, the $+c$ plane of AlInN exhibited a higher etching resistance than the $-c$ plane of GaN, and a very thin AlInN layer was sufficient for this etching technique, which would help decrease the series resistance of power devices.

Reverse-tapered edges were obtained along the entire circumference of the hexagonal mesa. Figures 4(b) and 4(b') and Figs. 4(c) and 4(c') show bird's-eye view SEM images of the GaN mesas after wet etching for 20 and 55 min, respectively. Undercut etching was clearly observed at the top-GaN/AlInN interface on the sidewalls. The protrusions at the vertices of the hexagons were also subjected to etching and were removed after 55 min to leave behind a GaN hexagonal mesa without protrusions. Some inverted pyramidal structures resembling stalactites appeared on the reverse-tapered facets, which have also been observed on wet-etched $-c$-face GaN surfaces.[26–28] A plausible reason for their formation is dislocations acting as preferential sites for the pyramidal etching process.[28] These undesirable inverse pyramids should be decreased by using low-dislocation-density GaN substrates grown in the liquid phase.[29]

The protrusions at the vertices were intentionally included in the patterned Ni mask to maintain the reverse-tapered structure at the vertices. Figure 5 shows SEM images of a vertex without a protrusion before [Fig. 5(a)] and after 20 and 55 min of wet etching [Figs. 5(b) and 5(c), respectively]. Because the sidewall of the vertex included an etching-vulnerable a-plane facet, the vertex was removed during the etching to form a positively tapered structure. Thus, a sacrificial structure (e.g. protrusion) directed in the a direction was necessary to avoid positive tapering of the vertex.

In conclusion, we demonstrated a state-of-the-art process for reverse tapering GaN on a lattice-matched AlInN layer. We successfully fabricated hexagonal GaN mesas with a reverse taper along their entire circumference. This structure can be applied to realizing positive beveled edge terminations for GaN power devices, which has not yet been demonstrated despite its effectiveness. We believe this fabrication process will greatly contribute to the development of high-performance GaN power devices.

Acknowledgments This work was supported by the TIA Kakehashi (TK23-001), and the "Advanced Research Infrastructure for Materials and Nanotechnology in Japan (ARIM)" initiative of the Ministry of Education, Culture, Sports, Science and Technology (MEXT), (JPMXP1224NM5062).

ORCID iDs Takayoshi Oshima https://orcid.org/0000-0001-8550-9735 Masataka Imura https://orcid.org/0000-0002-4236-9549 Yuichi Oshima https://orcid.org/0000-0001-8293-4891

1) T. J. Flack, B. N. Pushpakaran, and S. B. Bayne, J. Electron. Mater. **45**, 2673 (2016).
2) B. N. Pushpakaran, A. S. Subburaj, and S. B. Bayne, J. Electron. Mater. **49**, 6247 (2020).
3) J. He, W. Cheng, Q. Wang, K. Cheng, H. Yu, and Y. Chai, Adv. Electron. Mater. **7**, 2001045 (2021).
4) R. T. Yadlapalli, A. Kotapati, R. Kandipati, S. R. Balusu, and C. S. Koritala, Int. J. Energy Res. **45**, 12638 (2021).

5) H. Fu, K. Fu, S. Chowdhury, T. Palacios, and Y. Zhao, IEEE Trans. Electron Devices **68**, 3200 (2021).
6) K. Nomoto et al., 2015 IEEE Int. Electron Devices Meet. 2015 (IEEE), p. 9.7.1.
7) M. Matys et al., Appl. Phys. Express **14**, 074002 (2021).
8) V. Talesara, Y. Zhang, V. G. T. Vangipuram, H. Zhao, and W. Lu, Appl. Phys. Lett. **122**, 123501 (2023).
9) W. Lin, M. Wang, R. Yin, J. Wei, C. P. Wen, B. Xie, Y. Hao, and B. Shen, IEEE Electron Device Lett. **42**, 1124 (2021).
10) R. L. Davies and F. E. Gentry, IEEE Trans. Electron Devices **11**, 313 (1964).
11) B. J. Baliga, *Fundamentals of Power Semiconductor Devices* (Springer International Publishing, 2019) 2nd ed.
12) D. A. Stocker, E. F. Schubert, and J. M. Redwing, Appl. Phys. Lett. **73**, 2654 (1998).
13) T. Kaneko, K. Horino, H. Yamamoto, H. Ito, and A. Kuramata, J. Light Vis. Environ. **32**, 124 (2008).
14) C.-F. Lin, C.-M. Lin, C.-C. Yang, W.-K. Wang, Y.-C. Huang, J.-A. Chen, and R.-H. Horng, Electrochem. Solid-State Lett. **12**, H233 (2009).
15) Y.-C. Huang, C.-F. Lin, S.-H. Chen, J.-J. Dai, G.-M. Wang, K.-P. Huang, K.-T. Chen, and Y.-H. Hsu, Opt. Express **19**, A57 (2011).
16) R. Butté et al., J. Phys. D: Appl. Phys. **40**, 6328 (2007).
17) D. Simeonov, E. Feltin, A. Altoukhov, A. Castiglia, J. F. Carlin, R. Butt́, and N. Grandjean, Appl. Phys. Lett. **92**, 171102 (2008).
18) I. M. Watson, C. Xiong, E. Gu, M. D. Dawson, F. Rizzi, K. Bejtka, P. R. Edwards, and R. W. Martin, MEMS, MOEMS, Micromach. III **6993**, 69930E (2008).
19) M. Bellanger, V. Bousquet, G. Christmann, J. Baumberg, and M. Kauer, Appl. Phys. Express **2**, 121003 (2009).
20) A. Altoukhov, J. Levrat, E. Feltin, J.-F. Carlin, A. Castiglia, R. Butté, and N. Grandjean, Appl. Phys. Lett. **95**, 191102 (2009).
21) P. Sana, C. Seneza, C. Berger, H. Witte, M.-P. Schmidt, J. Bläsing, S. Neugebauer, F. Hoerich, A. Dadgar, and A. Strittmatter, Jpn. J. Appl. Phys. **60**, 010905 (2021).
22) M. Miyoshi, T. Nakabayashi, M. Yamanaka, T. Egawa, and T. Takeuchi, J. Vac. Sci. Technol. **B 38**, 052205 (2020).
23) M. Miyoshi, M. Yamanaka, T. Egawa, and T. Takeuchi, Appl. Phys. Express **11**, 051001 (2018).
24) S. J. Pearton, R. J. Shul, and F. Ren, MRS Internet J. Nitride Semicond. Res. **11**, 11 (2000).
25) H. Schulz and K. H. Thiemann, Solid State Commun. **23**, 815 (1977).
26) S. L. Qi et al., Appl. Phys. Lett. **95**, 071114 (2009).
27) Y. Jung, J. Ahn, K. H. Baik, D. Kim, S. J. Pearton, F. Ren, and J. Kim, J. Electrochem. Soc. **159**, H117 (2011).
28) L. Wang, J. Ma, Z. Liu, X. Yi, G. Yuan, and G. Wang, J. Appl. Phys. **114**, 133101 (2013).
29) D. Sun, L. Liu, G. Wang, J. Yu, Q. Li, G. Tian, B. Wang, X. Xu, L. Zhang, and S. Wang, Chem.—Eur. J. **30**, e202303710 (2024).